ARTICLE

Novel Electrospun Chitosan/PEO Membranes for More Predictive Nanoparticle Transport Studies at Biological Barriers

Lea A. Furer, [a,b] Ángela Díaz Abad, [a] Pius Manser, [a] Yvette Hannig, [a] Simone Schuerle, [b] Giuseppino Fortunato [c] and Tina Buerki-Thurnherr *[a]

The design of safe and effective nanoparticles (NPs) for commercial and medical applications requires a profound understanding of NP translocation and effects at biological barriers. To gain mechanistic insights, physiologically relevant and accurate human *in vitro* biobarrier models are indispensable. However, current transfer models largely rely on artificial porous polymer membranes for the cultivation of cells, which do not provide a close mimic of the natural basal membrane and intrinsically provide limited permeability for NPs. In this study, electrospinning is exploited to develop thin chitosan/polyethylene oxide (PEO) membranes with a high porosity and nanofibrous morphology for more predictive NP transfer studies. The nanofiber membranes allow the cultivation of a tight and functional placental monolayer (BeWo trophoblasts). Translocation studies with differently sized molecules and NPs (Na-fluorescein; 40kDa FITC-Dextran; 25 nm PMMA; 70, 180 and 520 nm polystyrene NPs) across empty and cell containing membranes reveal a considerably enhanced permeability compared to commercial microporous membranes. Importantly, the transfer data of NPs is highly similar to data from *ex vivo* perfusion studies of intact human placental tissue. Therefore, the newly developed membranes may decisively contribute to establish physiologically relevant *in vitro* biobarrier transfer models with superior permeability for a wide range of molecules and particles.

Introduction

There is a continuous increase of the presence of nanomaterials in our society. Nanoparticles do not only exist in nature[1, 2] or arise as unintended by-products from industrial processes, combustion and traffic[3], but are also specifically designed and engineered for industrial[4], commercial[5, 6] or medical[7] applications. The European Commission defines nanomaterials as materials where at least one dimension is smaller than 100 nm.[8] This small size comes with many beneficial properties, such as a large surface to volume ratio, increased reactivity or enhanced hardness and magnetic, electric or antibacterial properties.[4] These traits have led to a widespread use of such nanomaterials. To mention some examples, titanium dioxide and zinc oxide particles are efficient UV filters in sunscreens.[4, 6] Amorphous silica (E551) serves as anticaking agent in food products.[5] Gold nanoparticles are used in diagnostic tools.[4] Magnetic nanoparticles can help to treat cancer with magnetic hyperthermia.[9, 10] Iron oxide nanoparticles serve as contrast agents in magnetic resonance imaging.[11] Various metallic or polymeric NPs are exploited as efficient drug delivery vehicles, and silver NPs are popular for their antimicrobial properties.[7]

Therefore, exposure of humans and the environment to NPs is unavoidable and raises safety concerns. It is known that NPs can cross a variety of primary outer tissue barriers such as the skin, lung or intestine[12-14], and are also able to overcome various internal barriers, such as the blood-brain[15-17], the blood-testis[17, 18] and the blood-placenta[17, 19] barriers. The presence of NPs in the tissue can lead to the formation of reactive oxygen species (ROS), triggering oxidative stress, inflammation and genotoxicity[20], which may result in severe side effects. Consequently, a careful risk assessment of NP exposure is required, and studies dealing with the translocation and effects of NPs at the different biological barriers are particularly important to estimate systemic exposure and biodistribution in the body. It is crucial to understand which NPs are able to cross certain barriers, to identify the underlying translocation mechanisms and to assess the influence of different NPs on biobarrier integrity and function. For these purposes, physiologically relevant and reliable model systems are required. Animal models have been used to study the transport and effect of NPs at biological barriers in an intact organism, but there are considerable uncertainties in the extrapolation of the results to humans due to species-specific differences[13] as well as limitations to perform mechanistic transfer studies. Human ex vivo or precision cut tissue slice culture models, in contrast, deliver more predictive results, but the restricted access to human tissues, a low throughput or poor penetration of NPs into tissue slices limit the broad application of such methods.[21,22] Therefore, predictive and human relevant in vitro biobarrier models are indispensable and of high value for the

a. *Empa, Swiss Federal Laboratories for Materials Science and Technology, Laboratory for Particles-Biology Interactions, 9014 St. Gallen, Switzerland*
b. *ETH Zürich, Responsive Biomedical Systems Lab, 8093 Zürich, Switzerland*
c. *Empa, Swiss Federal Laboratories for Materials Science and Technology, Laboratory for Biomimetic Membranes and Textiles, 9014 St. Gallen, Switzerland ddress here.*

initial screening of a vast variety of engineered and environmental NPs to estimate barrier crossing and toxicity and to generate mechanistic insights on structure-activity relationships.

In vitro, the natural tissue architecture is mimicked by culturing the key cell types of the tissue barrier, usually epithelial and endothelial cells, on opposite sides of a microporous track-etched polymer membrane to form a two-compartment model. To recapitulate the dynamic situation in the body, several groups have also integrated such membranes in more complex tissue-on-chip models, where fluidic shear stress and mechanical stretching can be applied to provide a more physiological microenvironment to the cells.[23-25] However, most microfluidic devices are made out of polydimethylsiloxane (PDMS), which is known to absorb small hydrophilic molecules.[26-28] This drawback could impede reliable and predictive drug and NP transfer studies. Moreover, the commercial track-etched membranes suffer from several innate and interfering limitations for NP transfer studies such as low porosity, particle absorption or high thickness, which prevents a predictive risk assessment of NP transport and effects at biological barriers. While track-etched membranes are highly permeable to small drugs and molecules, their innate characteristics can considerably limit the diffusion of macromolecules and NPs across the empty membrane without cells.[29, 30] Therefore, the use of low permeability membranes could underestimate transfer rates or even fail to detect a low NP transport. As an example, it has been shown that placental transport of 50 nm polystyrene (PS) NPs reached 35% of the initial dose after 3 h in the ex vivo placenta perfusion model[31], while only 1-2% of the applied particles were reaching the basolateral compartment in an in vitro placental transfer model even upon extended exposure for 24 h.[32] Therefore, a redesign of porous membrane supports is urgently needed.

A promising technique to fabricate highly permeable membranes is electrospinning.[33, 34] A key advantage of this technique is that the resulting membranes are made of micro- or nanofibers that mimic the structure of the natural basement membrane. Additionally, they exhibit a large surface-to-volume ratio and high porosity[33], which is expected to achieve more physiologic transport rates of NPs. Furthermore, the electrospinning process is simple, versatile, cost-effective, scalable and tunable. In 2017, a first proof-of-concept study successfully established electrospun membranes for a co-culture alveolar-capillary barrier model.[35] Higher permeability was achieved for small molecules, however, the membranes were not yet optimized and validated for the evaluation of NP transfer and associated effects.

In this study, we report the development of novel electrospun nanofibrous chitosan/PEO membranes with a high porosity for more predictive NP transport studies at biological barriers. After removal of the original membrane of a commercially available ce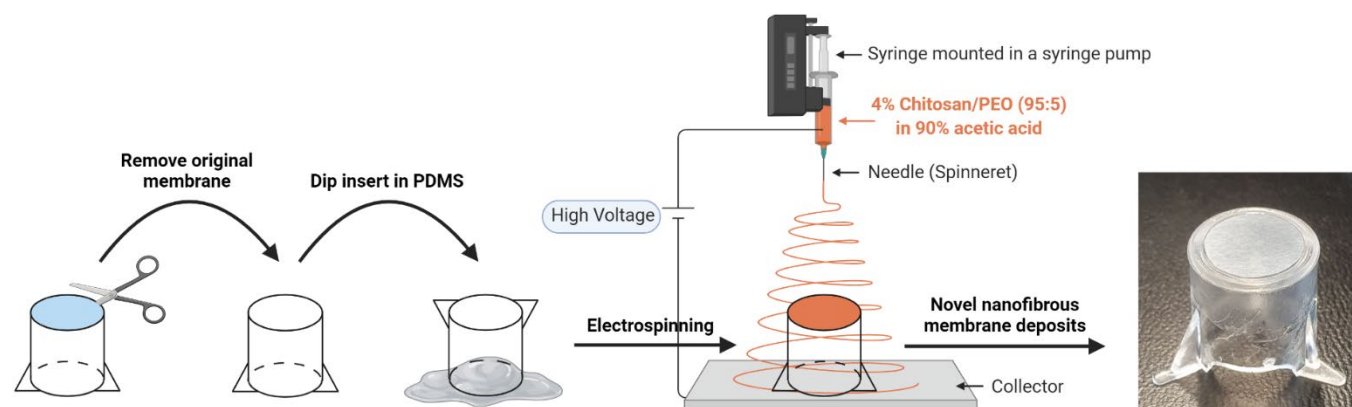ll culture insert, the membranes were electrospun directly onto the insert carriers. Chitosan was used because it is a natural, highly abundant biopolymer[36] with many beneficial properties such as biocompatibility[37], biodegradability[38], non-antigenicity[37], cytocompatibility towards various cell types[39] and inherent antimicrobial effects[40]. Therefore, it has already been used in various tissue engineering applications.[41] Since chitosan is rather difficult to electrospin, it is often blended with other polymers such as PEO that reduces the viscosity and improves the stability of the spinning process.[36, 42] PEO is a highly biocompatible synthetic polymer approved for use in pharmaceuticals, food, cosmetics and personal care products.[36] After a comprehensive characterization of the newly developed membranes, we established a tight placental barrier using the BeWo b30 trophoblast cell line on the inserts. We decided to focus on the placenta because pregnant women and the developing fetus are particularly vulnerable and evidence is increasing that exposure to engineered or environmental NPs could be of particular concern and involved in the development of diseases later in life.[43] In humans, the placenta is a transient organ which develops during pregnancy and has many important functions such as the exchange of nutrients and oxygen for carbon dioxide and waste products, the protection of the fetus and the production of pregnancy hormones.[44] It is assumed that developmental toxicity is not only induced from translocated NPs but could also have a placental origin if NP induce negative effects on placental tissue viability and functionality or lead to the release of inflammatory, vascular or endocrine mediators that indirectly impair fetal development.[45, 46]

Once a tight trophoblast barrier was formed on the insert, we conducted several translocation studies with small molecules (sodium fluorescein (Na-F); 40 kDa FITC-Dextran) and differently sized NPs (25 nm PMMA; 70, 180 and 520 nm PS NPs). We compared the data to results obtained from ex vivo placenta perfusion studies to highlight the improved permeability and predictive value of the newly developed membranes.

Results

Membrane fabrication and characterization

Chitosan/PEO membranes were electrospun directly on cell culture inserts from a 4% chitosan/PEO solution (95:5 w/w) in 90% acetic acid. The polymer solution showed a shear-thinning behavior (Figure S1) and a conductivity of 431.6 ± 20.2 μs cm^{-1} and was therefore well suited for electrospinning. The fabrication process of the membranes is shown in Figure 1. First, the original membrane of a commercial ThinCert® cell culture insert was removed and the upper ring of the insert was dipped in a liquid PDMS solution. This thin PDMS layer is required to glue the new membrane tightly to the insert. Then, electrospinning was performed and a freestanding uniform nanofibrous membrane was deposited on the insert.

Figure 1. Fabrication of free-standing chitosan/PEO membranes on cell culture inserts. First, the original membrane of a commercial ThinCert® cell culture insert was removed and the insert was dipped in a liquid PDMS glue. Then, electrospinning was performed at ambient conditions and a free-standing nanofibrous membrane deposited on the insert. Figure created with Biorender.com.

Afterwards, the membranes were crosslinked for 4 h in glutaraldehyde (GA) vapor and subsequently dried for at least 24 h in a vacuum oven at 40 °C to remove remaining GA residues and harden the PDMS.

We tested two different electrospinning durations, 2 min and 4 min, to investigate the hypothesis that longer spinning times lead to thicker membranes with a reduced porosity and pore size. The resulting membranes were thoroughly characterized and compared to commercial ThinCert® membranes. Scanning electron microscopy (SEM) images revealed that the electrospun fibers deposited uniformly across the cell culture insert (Figure 2a,b,d,e). Before crosslinking, the average fiber diameter was 273.2 ± 79.0 nm. After crosslinking for 4 h in glutaraldehyde, the fiber diameter slightly increased to 312.8 ± 88.6 nm. When the crosslinked membranes were immersed in phosphate-buffered saline (PBS) for 5 days, the nanofibrous structure was preserved and only minimal swelling occurred (average fiber diameter 339.3 ± 95.5 nm). However, a few fused fibers could be observed and some salt crystals deposited on the membrane (Figure S2). In contrast, the commercial ThinCert® membranes exhibited a flat surface structure with randomly distributed spherical pores (Figure 2g,h). To determine the hydrophilicity of the membranes, water contact angle (WCA) measurements were performed. The 2 min and 4 min chitosan/PEO membranes showed very similar WCA of 45.9 ± 7.2° and 48.4 ± 2.4°, respectively while the ThinCert® membranes had a WCA of 83.6 ± 8.8°. Thus, although none of the membranes were hydrophobic, the chitosan/PEO membranes exhibited a superior hydrophilicity. The pore size was determined from SEM images and the pore size distribution is shown in Figure 2k. While ThinCert® membranes had uniform 3 µm pores, the electrospun membranes presented pores of various sizes due to the random organization of the nanofibers. As hypothesized, electrospinning duration affected the pore size. For the 2 min membranes, the vast majority of pores was smaller than 4 µm, with a few single pores that reached a larger

size of up to 5.7 µm. For the 4 min membranes, most of the pores were smaller than 2 µm, and the largest measured pore had a size of 2.73 µm. The median values were 1.13 µm and 0.72 µm for the 2 min and 4 min membranes, respectively.

Since the chitosan/PEO membranes exhibited fluorescent properties, we determined the thickness of the membranes from reconstructed three dimensional confocal laser scanning microscope (CLSM) micrographs (Movie S1 & S2). The thickness of 2 min and 4 min chitosan/PEO membranes were 3.6 ± 0.9 µm and 6.9 ± 0.8 µm, respectively (p-value < 0.01). In contrast, the commercial ThinCert® membranes exhibited a thickness of 10 µm (Figure 2l). The porosity was 62.9 ± 4.2% for the 2 min and 39.3 ± 3.7% for the 4 min chitosan/PEO membranes (p-value < 0.01), but only 14.1% for the ThinCert® membranes (Figure 2j).

Additionally, we performed first translocation studies across cell-free membranes to compare their permeability. Differently sized molecules and NPs (Na-F, 40 kDa FITC-Dextran, 25 nm PMMA NPs and 70, 180 & 520 nm PS NPs) covering a wide size range were applied to the apical compartment and the amount that reached the basolateral compartment was measured at different time points. As expected, the results showed that the 2 min chitosan/PEO membranes were significantly more permeable than the 4 min chitosan/PEO membranes (for Na-F, 40 kDa FITC-Dextran, 180 nm PS and 520 nm PS; p-value < 0.001 for all these conditions) or the ThinCert® membranes (for 70 nm, 180 nm and 520 nm PS; p-value always < 0.001) (Figure S3b,c,d,f,g,h).

Collectively, the characterization data indicated that the 2 min chitosan/PEO membranes were a promising candidate to fabricate novel cell culture membrane supports with a superior permeability to a wide range of molecules and particles. Since shorter electrospinning durations (< 2 min) resulted in too fragile membranes with too large pores for culturing cell monolayers, we selected 2 min electrospinning for our further experiments.
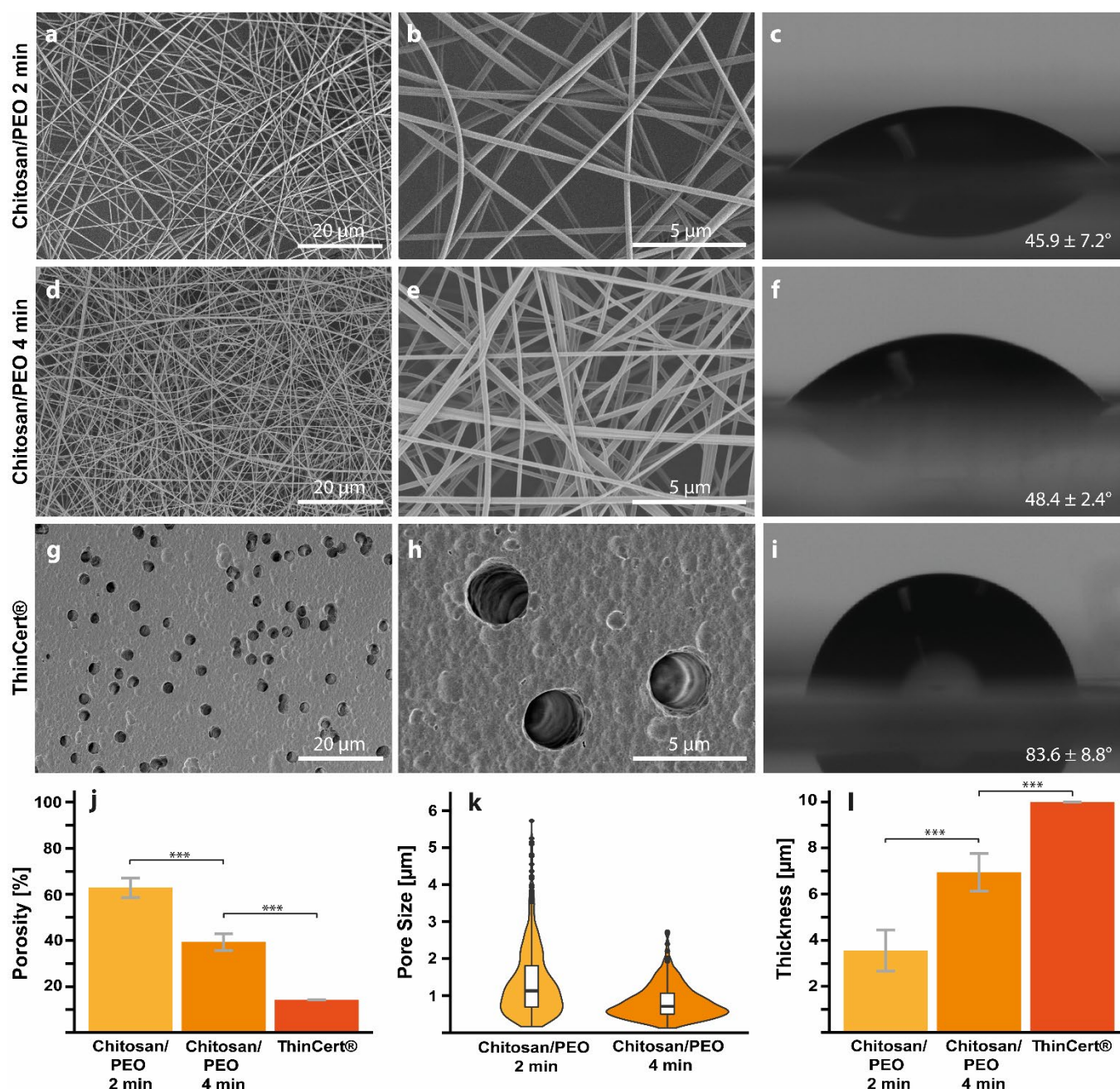
Figure 2. Membrane characterization. The chitosan/PEO and ThinCert® membranes were characterized by SEM with a 1.5k (a, d, g) and 8k (b, e, h) magnification, and their water contact angle was determined (c, f, i). Porosity (j), pore size distribution (k) and thickness (l) of the chitosan/PEO membranes were measured and compared with the corresponding values of the ThinCert® membranes (for porosity and thickness only). The data in figure (j) and (l) represent mean ± STD from 6 different chitosan/PEO membranes per condition, or values supplied by the manufacturer (for ThinCert® membranes). *** p-value < 0.001

### Establishment and characterization of a human placental trophoblast barrier

To exploit the suitability of chitosan/PEO membranes for in vitro cell barrier cultures, we chose to recreate a functional human placental trophoblast barrier. An advantage of this model is that we can verify in vitro transfer rates against data from perfusion of an isolated lobule of human term placenta.[44] For this, human BeWo b30 trophoblast cells were grown on the apical side of

ThinCert® or 2 min chitosan/PEO membranes. Using previously established culture conditions[32], we confirmed the formation of a tight BeWo monolayer on ThinCert® membranes 3 days after seeding of 1.5×10^5 cells (Figure S4). To find optimal culture conditions for the 2 min chitosan/PEO membranes, different cell seeding numbers of 1.5×10^5, 2×10^5, 2.5×10^5 and 3×10^5 cells/membrane were applied and barrier formation and integrity was monitored. To form a tight cell barrier, 2.5×10^5 cells/membrane were required. With this cell seeding number, Immunocytochemistry (ICC) staining showed that a confluent

cell monolayer covered the whole membrane area (Figure 3a,d) and the cells expressed adherens junctions (γ-catenin staining; Figure 3b) and tight junctions (ZO-1 staining; Figure 3c). Transepithelial electrical resistance (TEER) values increased over time and reached $149.7 \pm 54.2\ \Omega\ cm^{-2}$ at day 3 and $297.4 \pm 114.4\ \Omega\ cm^{-2}$ at day 4 (Figure 3e). Na-F and 40 kDa FITC-Dextran translocation decreased significantly after 72 h (basolateral amount of Na-F $14.5 \pm 14.2\%$ of initial dose (ID) (p-value < 0.001), basolateral amount of FITC-Dextran $9.7 \pm 8.0\%$ of ID (p-value < 0.01), as shown in Figure 3f,g. However, when lower cell numbers were used, the cell layers were not confluent and Na-F and FITC-Dextran translocation was increased (Figure S5 & Figure S6).
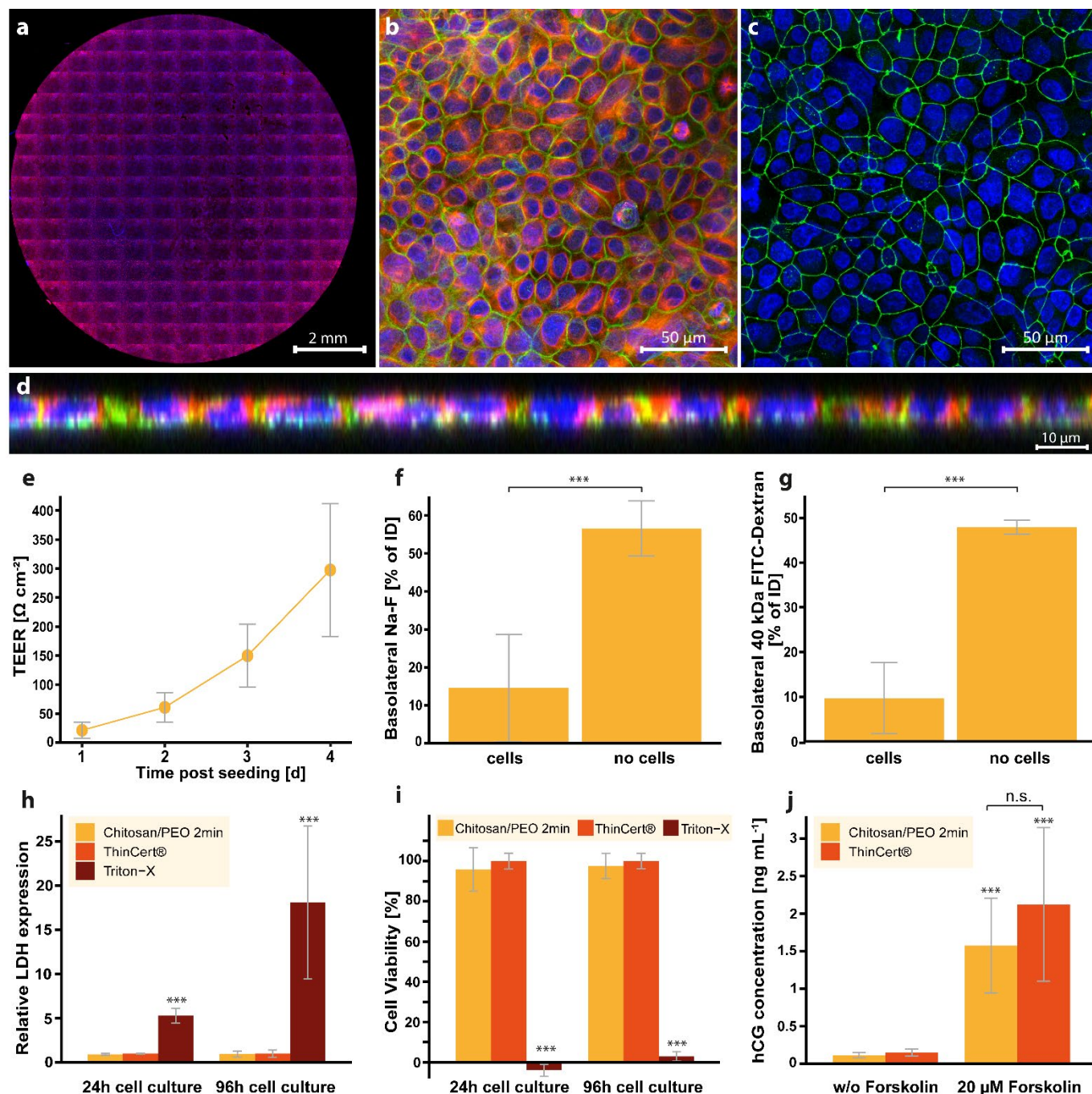
Figure 3. Formation of a tight placental trophoblast barrier on chitosan/PEO membranes. ICC staining of BeWo b30 cells on chitosan/PEO membranes (a-d). 2.5×10^5 cells/membrane were seeded and cultured for 72 h. Whole membrane is shown in (a). Cell nuclei (Dapi; blue) and tubulin (red) are stained. (b) CLSM image showing tubulin (red), adherens junctions (γ-catenin; green) and cell nuclei (Dapi; blue). (c) CLSM image showing cell nuclei (Dapi; blue) and tight junctions (ZO-1; green). (d) CLSM cross-section (blue = Dapi, red = tubulin, green = γ-catenin). Barrier formation was determined by TEER measurements (e) and Na-F (f) and 40 kDa FITC-Dextran (g) exclusion assays. LDH (h) and MTS (i) assays and an hCG ELISA (j) were performed to assess cell viability and functionality. Data represents mean ± STD from at least 3 independent experiments with 2 technical replicates each. *** p-value < 0.001 compared to the untreated control samples.
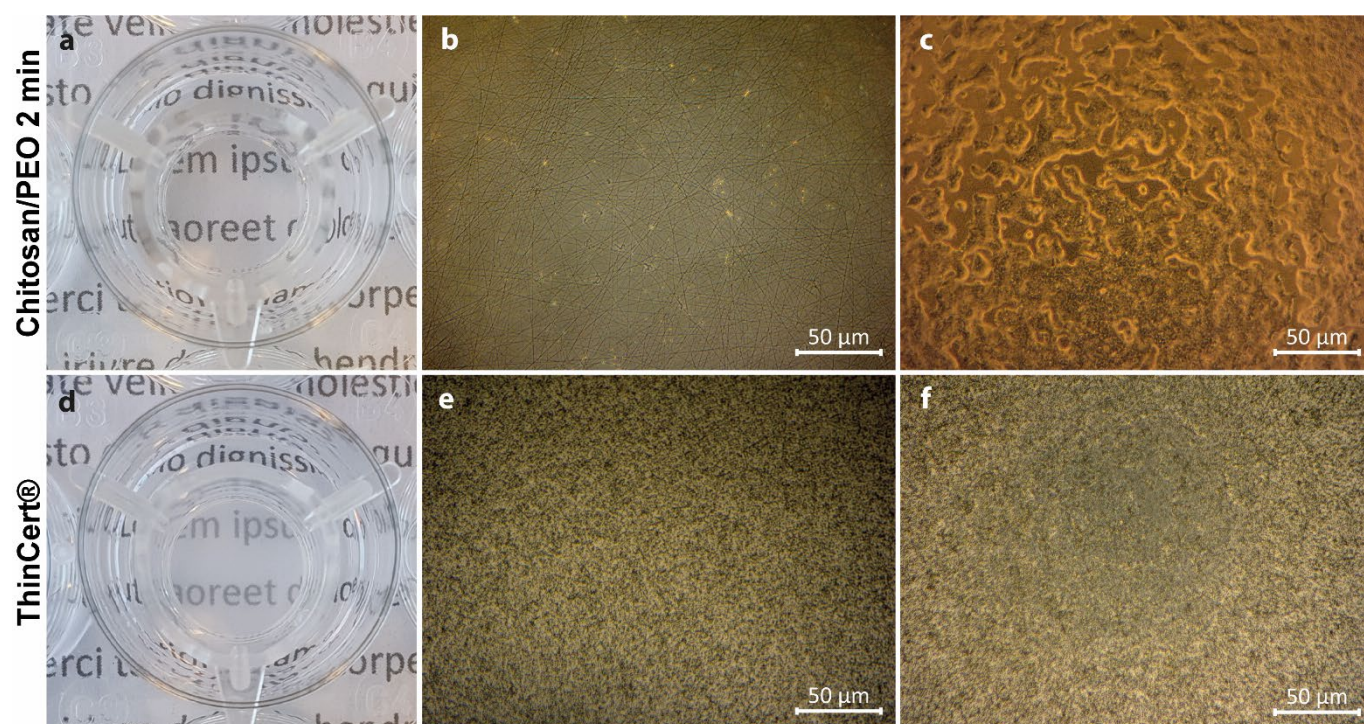
Figure 4. Optical transparency. Optically transparent 2 min chitosan/PEO (a) and translucent ThinCert® (d) membranes immersed in PBS. Light microscopy image of empty membranes (b & e) and membranes with cultured BeWo b30 cells (c & f).

In contrast, when higher cell numbers were seeded or cells were cultured for a longer time period of 96 h, cell overgrowth and multilayer formation was observed (Figure S7). Therefore, a cell seeding number of 2.5×10^5 cells and a culture duration of 72 h were selected for further experiments.

In a next step, we assessed cell viability and functionality of the BeWo cells. There were no relevant differences in lactate dehydrogenase (LDH) release and mitochondrial activity between cells cultured on chitosan/PEO or ThinCert® membranes (Figure 3h,i). Additionally, cells on chitosan/PEO and ThinCert® membranes had similar human chorionic gonadotropin (hCG) levels and hCG production could be stimulated by the addition of 20 µM forskolin, which is a known inducer of trophoblast differentiation (Figure 3j). These results confirmed that BeWo cells grown on chitosan/PEO membranes were highly functional.

Additionally, the chitosan/PEO membranes exhibited a superior transparency compared to existing cell culture membranes. NP transport studies require inserts with a large pore size and high pore density, and track-etched membranes fulfilling these criteria are often not transparent enough to observe the cells under a light microscope. For example, we could not distinguish between empty and cell-containing ThinCert® polyethylene terephthalate (PET) membranes with 3 µm pores (Figure 4e,f), while cells could easily be detected and observed when grown on chitosan/PEO membranes (Figure 4b,c).
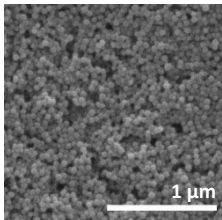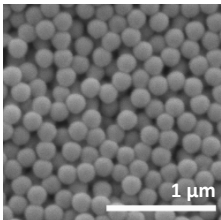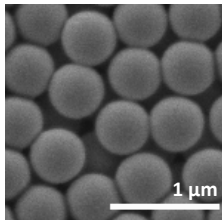
Translocation of small molecules and NPs

The permeability of the newly developed BeWo transfer model on chitosan/PEO membranes was investigated by conducting translocation studies with differently sized molecules and NPs. Before conducting these experiments, the NPs were characterized and their hydrodynamic size and surface charge were measured. Additionally, SEM micrographs confirmed the spherical shape and primary particle size of the NPs (Table 1).

Table 1. Summary of NP characteristics.

	25 nm PMMA	70 nm PS	180 nm PS	520 nm PS
Primary particle size[a]	25 nm	70 nm	180 nm	520 nm
Hydrodynamic size in 10% PBS [nm][b]	42.8 ± 0.5 (PdI: 0.199 ± 0.012)	224.4 ± 13.5 (PdI: 0.252 ± 0.006)	185.8 ± 2.1 (PdI: 0.071 ± 0.025)	538.7 ± 11.4 (PdI: 0.062 ± 0.038)
Hydrodynamic size in EC media [nm][b]	41.7 ± 0.3 (PdI: 0.294 ± 0.027)	147.1 ± 0.9 (PdI: 0.203 ± 0.016)	239.6 ± 3.9 (PdI: 0.129 ± 0.019)	658.6 ± 18.3 (PdI: 0.116 ± 0.033)

Zeta potential in 10% PBS [mV][b]	-14.8 ± 1.3	-29.1 ± 0.9	-68.2 ± 2.9	-87.4 ± 4.1
SEM Image	Not possible to detect NPs with SEM	1 µm	1 µm	1 µm

a) Data supplied by the manufacturer; b) Experimentally determined: Hydrodynamic diameter in 10% PBS and EC media (data shows mean ± STD of 5 consecutive runs). Zeta potential in 10% PBS (data shows mean ± STD). Abbreviations: PBS; phosphate buffered saline.

Cells were cultivated for 72 h on 2 min chitosan/PEO and ThinCert® membranes before they were incubated with 5 µM Na-F (376 Da), 5 µM FITC-Dextran (40 kDa) or fluorescently labeled 0.5 mg mL⁻¹ 25 nm PMMA, 50 µg mL⁻¹ 70 nm, 50 µg mL⁻¹ 180 nm or 50 µg mL⁻¹ 520 nm PS. The translocation of the differently sized molecules and particles to the basolateral compartment was determined at various time points during 24 h (Table 2, Figure 5). These transfer studies confirmed a size dependent transport with higher transfer rates for smaller molecules/particles across empty membranes or BeWo trophoblast barriers.

Electrospun chitosan/PEO membranes were more permeable than the commercial track-etched ThinCert® membranes, especially for larger molecules and NPs. For cell free membranes, significant differences in permeability were obtained for 70 nm, 180 nm and 520 nm PS particles (p-value < 0.001 for all these conditions). In the presence of a confluent BeWo layer, significant differences in the permeability appeared already for 40 kDa FITC-Dextran (p-value = 0.003) and 25 nm PMMA particles (p-value < 0.001) and were also present for the larger (70 nm (p-value < 0.001) , 180 nm (p-value < 0.001), 520 nm (p-value = 0.003)) PS NPs.

The superior permeability of the chitosan/PEO membranes was not only apparent from the increased translocated amount of molecules and particles after 24 h but was also reflected in the transfer kinetics (Figure 5). For instance, equilibrium concentrations for Na-F were reached earlier across empty chitosan/PEO membranes (4 h) than across empty ThinCert® membranes (8 h). For 40 kDa FITC-Dextran and 25 nm PMMA particles, an equilibrium was reached after 24 h only for the empty chitosan/PEO membranes. However, the larger PS NPs did not reach equal concentrations in the two compartments within 24 h, regardless of the membrane type used. Moreover, when summing the apical and basolateral particle counts, a loss of PS particles was evident, which was particularly pronounced for larger particles and could be observed for both cell-free membranes and tight BeWo barriers. Therefore, we investigated whether the NPs were absorbed by the membranes and/or taken up by the cells. CLSM analysis confirmed that the larger PS NPs (≥ 70 nm) could be found in the membranes (for cell-free conditions) or the placental BeWo cells (Figure S8).

Table 2. Translocation rates of different sized molecules and NPs across chitosan/PEO or ThinCert® membranes in presence and absence of a BeWo trophoblast layer after 24 h.

Molecule/NP	Translocation rates for chitosan/PEO [% of ID]	Translocation rates for ThinCert® [% of ID]
Na-F	Empty membrane: 79.2 ± 11.6% With cells: 59.6 ± 16.2%	Empty membrane: 79.0 ± 8.0%, With cells: 43.8 ± 17.2%
40 kDa FITC-Dextran	Empty membrane: 74.3 ± 6.8% With cells: 38.6 ± 23.8%	Empty membrane: 67.6 ± 6.4% With cells: 12.6± 8.9%
25 nm PMMA	Empty membrane: 71.5 ± 9.2% With cells: 46.1 ± 13.7%	Empty membrane: 64.2 ± 7.4% With cells: 23.2 ± 5.1%
70 nm PS	Empty membrane: 63.1 ± 8.8% With cells: 23.6 ± 15.9%	Empty membrane: 32.5 ± 10.5% With cells: 6.9 ± 3.4%
180 nm PS	Empty membrane: 54.1 ± 8.4% With cells: 32.9 ± 16.7%	Empty membrane: 27.1 ± 9.1% With cells: 2.1 ± 2.1%
520 nm PS	Empty membrane: 51.6 ± 7.5% With cells: 18.1 ± 13.5%	Empty membrane: 35.3 ± 11.2%, With cells: 3.1 ± 1.7%
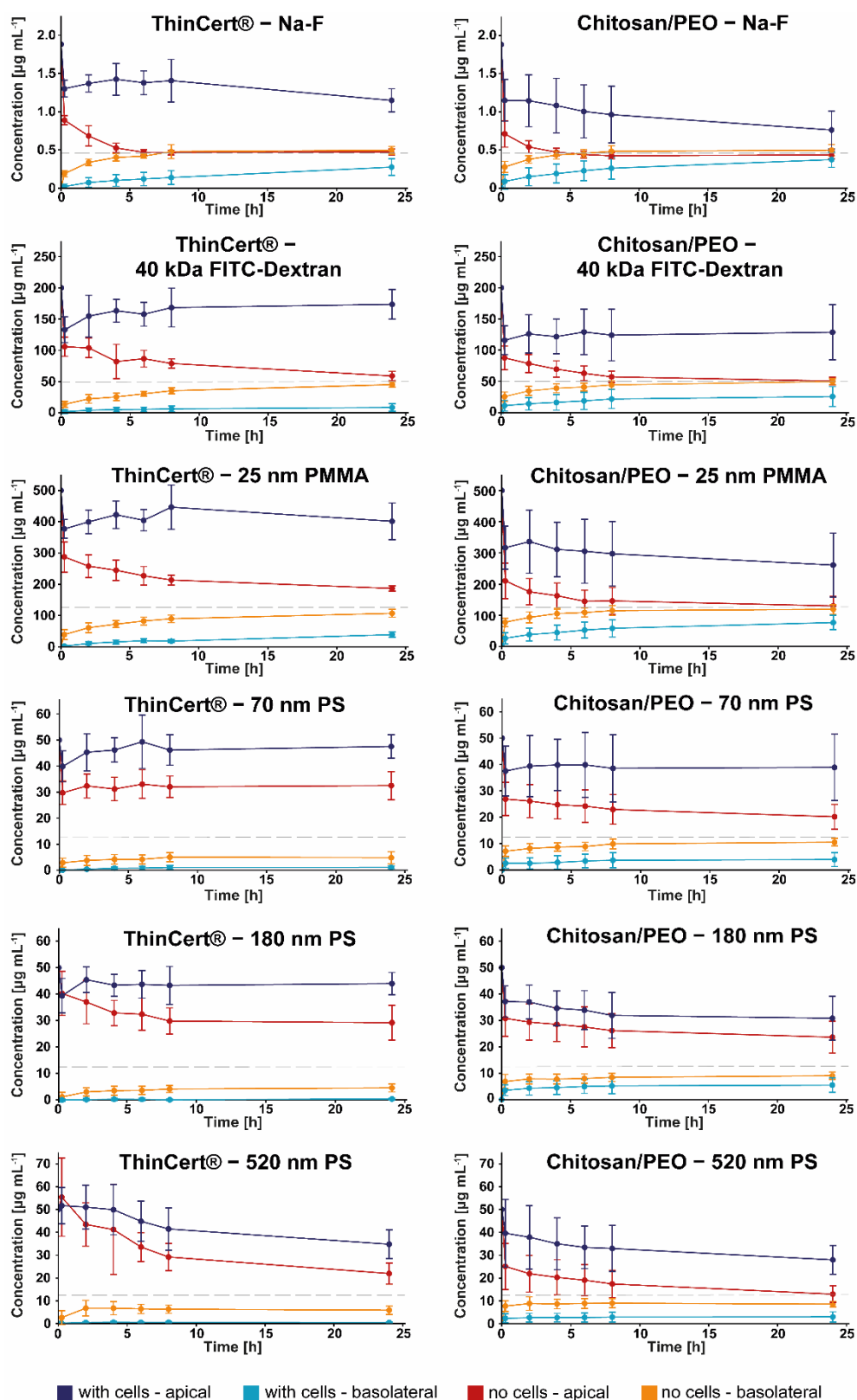
Figure 5. Translocation of differently sized molecules and particles across chitosan/PEO or ThinCert® membranes in presence and absence of a BeWo trophoblast barrier. Translocation of 1.9 µg mL^{-1} Na-F, 200 µg mL^{-1} FITC-Dextran (40 kDa), 0.5 mg mL^{-1} 25 nm PMMA, 50 µg mL^{-1} 70 nm PS, 50 µg mL^{-1} 180 nm PS and 50 µg mL^{-1} 520 nm PS across BeWo monolayers cultured on 2 min chitosan/PEO (right column) or ThinCert® (left column) membranes. Cells were cultivated for 72 h on collagen-coated inserts before translocation studies were performed. Data represents mean ± STD of 3 (ThinCert®) or 5 (chitosan/PEO) independent experiments with 3 technical replicates each. Cell-free membranes were included as a control. The dashed grey line shows the equilibrium concentration.
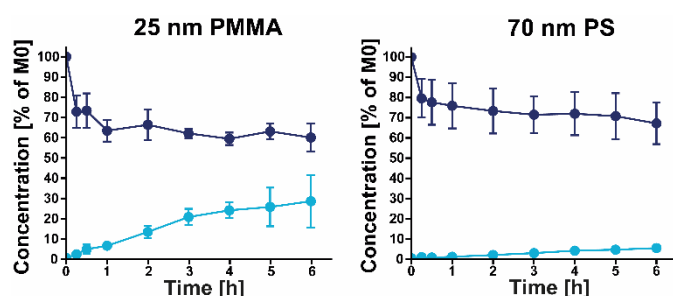
Figure 6. Ex vivo perfusion of human term placenta. The curves show the translocation profile of 25 nm PMMA and 70 nm PS NPs from the maternal to the fetal circulation. Results are expressed as mean ± STD of the initially applied concentration [M0] and represent the data from 3 independent perfusions.

Although the results from the translocation studies clearly indicate that the electrospun chitosan membranes are more permeable than their commercial counterparts, they do not yet allow any statement about the predictive value of the novel placental transfer model system. We therefore verified our model against the current gold standard ex vivo placenta perfusion model, which recapitulates near physiological conditions without any artificial membrane support and has been shown to provide highly predictive transport rates.[44] Because ex vivo placenta perfusion studies are technically demanding and time consuming, we focused on those NPs where we would expect a significant NP transfer to the fetal circulation. According to Wick et al., particles < 200 nm are able to cross the placental barrier, while larger NPs could barely be detected in the fetal compartment.[31] Therefore, we decided to conduct ex vivo placenta perfusion experiments with the 25 nm PMMA and 70 nm PS particles..

Figure 6 shows the results from our ex vivo perfusions. After 6 h, transfer rates for 25 nm PMMA and 70 nm PS were 28.4 ± 12.9% and 5.5 ± 0.3%, respectively, confirming that the smaller 25 nm PMMA NPs exhibited higher translocation rates, which is in line with previous findings of a size-dependent placental transport for PS NPs[47, 48].

Finally, Table 3 compares the ex vivo perfusion data with the results of our in vitro translocation studies. The results from the chitosan/PEO membranes (10.6 ± 5.1% for 25 nm PMMA; 5.5 ±

5.1% for 70 nm PS) were in better agreement with the data from ex vivo perfusion studies (28.4 ± 12.9% for 25 nm PMMA; 5.5 ± 0.3% for 70 nm PS), while ThinCert® membranes considerably underestimate placental NP transfer (3.9 ± 1.3% for 25 nm PMMA; 1.8 ± 1.3% for 70 nm PS).

Discussion

With the growing use of nanotechnology in our society, studies dealing with NP safety are becoming increasingly important. Especially a comprehensive knowledge on NP uptake and translocation mechanisms at different tissue barriers is of key importance for the safe design of NPs for industrial, commercial and medical applications. Therefore, predictive in vitro model systems for NP-biobarrier interaction and transfer studies are required, in particular since the predictive power of in vivo models is limited due to species differences. This is especially true for the human placenta, which is considered to be the most species-specific organ.[49] Complex ex vivo human placenta perfusion models exist and deliver predictive results, but a limited access to human placental tissue and a relatively low success rate limit their applicability for mechanistic translocation studies. Therefore, predictive in vitro alternatives are needed. In the most frequently used transfer system, cells are cultivated on cell culture inserts with a track-etched polymer membrane to form a two-compartment barrier model. However, these artificial scaffolds exhibit low permeability for NPs, probably due to their relatively high thickness (~10 μm) and low porosity. This prevents a predictive risk assessment. Therefore, research efforts have been made to optimize the porous membrane support for cell culture models (for a comparison of the available cell culture scaffolds including our newly developed membrane see Table S1). For example, ultrathin transparent SiO_2 or silicon nitride membranes with a thickness of 300 − 500 nm have been developed[50, 51] and showed a higher permeability to gold NPs[51] than track-etched PET membranes. However, these membranes are expensive, brittle and difficult to handle, which prevents their widespread use for NP screening experiments.

Table 3. **In vitro translocation vs. ex vivo perfusion.** Fetal (ex vivo) or basolateral (in vitro) concentration [% of initial concentration] after 6 h. Data represents mean ± STD of 3 independent experiments with 1 (ex vivo) or 3 (in vitro) technical replicates.

Nanoparticle	Ex vivo placenta perfusion	In vitro with Chitosan/PEO	In vitro with ThinCert®
25 nm PMMA	28.4 ± 12.9%	10.6 ± 5.1%	3.9 ± 1.3%
70 nm PS	5.5 ± 0.3%	5.5 ± 5.1%	1.8 ± 1.3%

Additionally, the artificial surface topography and material composition does not mimic the in vivo situation, where an ultrathin basement membrane (BM) separates the different cell types. The BM is a 50 to few hundred nm[52, 53] thin, nanofibrous and porous sheet of specialized extracellular matrix (ECM) proteins (pore size 10 nm to few μm[53, 54]) that provides

structural support, influences cell adhesion, migration and proliferation and acts as a selective barrier.[52, 55, 56] Therefore, other methods have been implemented to construct more physiologically relevant membranes. For example, Mondrinos et al. used different steps of vitrification to transform three-dimensional (3D) ECM hydrogels into structurally stable and

transparent films.[57] These ECM-derived membranes are inexpensive and mimic the architecture of the natural BM, but exhibit a limited permeability to larger molecules[57] and are therefore not suited for NP transport studies.

In this study, we aimed to design an inexpensive, highly permeable and biomimetic membrane support for predictive NP-biobarrier transfer and interaction studies. For this purpose, we employed electrospinning, an inexpensive, scalable and tunable process that allows the fabrication of highly porous, nanofibrous membranes, which mimic the structure of the natural ECM. As polymer combination, we chose a 4% chitosan/PEO (95:5 w/w) solution in 90% acetic acid, because previous studies in our lab ([36] and unpublished results) have shown its suitability for electrospinning, biocompatibility and potential for biomedical applications.

We successfully established chitosan/PEO membranes with a fiber diameter of 312.8 ± 88.6 nm, a thickness of 3.6 μm and a porosity of ~63% by direct electrospinning on insert holders. This is a remarkable improvement compared to traditional track-etched membranes (thickness of 10 μm; porosity of 1-14%) or vitrified ECM membranes (~20 μm thickness[57]). Additionally, most of the pores of the novel electrospun membrane had a pore size in the range from a few hundred nanometers to 4 μm. This is ideal for NP transfer studies, where pore sizes should be smaller than ~ 4-8 μm in order to prohibit cell migration but as large as possible to allow for efficient NP crossing (e.g. 0.4 μm pores can already extensively restrict transfer of 37 nm polystyrene NPs[58]). Moreover, the newly developed membranes are optically transparent when immersed in cell culture liquids, which allows monitoring of cell growth with a simple optical microscope.

To model the placental barrier in vitro, we established a confluent monolayer of BeWo trophoblast cells on the new chitosan/PEO membranes. In humans, the placental barrier is around 5 μm thick at the end of pregnancy and consists of a syncytiotrophoblast (STB) layer, its basal lamina that is partially covered with cytotrophoblast (CTB) cells and fetal endothelial cells on the opposite side of the basement membrane.[59] The CTB layer was omitted since it considerably thins after the first trimester and has been suggested to play a negligible role in substance transfer via the syncytium.[60] Furthermore, we did not include the endothelial cells for this study, since previous work indicated that NPs are often retained in the trophoblast layer[61-63] and the barrier capacity of a placental trophoblast monolayer to NPs was equal to the one of a co-culture with trophoblast cells and placental microvascular endothelial cells (HPEC).[32] Among the different trophoblast cell lines that are available, the BeWo b30 clone derived from a human malignant choriocarcinoma was favored, because it best resembles the in vivo STB structure and function.[64-66] Furthermore, it has been demonstrated that the relative transfer rates of small molecules measured in monolayer BeWo models correlate well with data obtained from ex vivo placenta perfusion.[32, 67, 68] We verified the biocompatibility of the electrospun membranes for cell viability and functionality (inducible hCG secretion in response to forskolin) and achieved to form a tight BeWo monolayer on the chitosan/PEO membranes, as verified by Na-F and 40 kDa FITC-

Dextran exclusion assays, TEER measurements and ICC stainings. However, the measured absolute TEER values were lower for cells cultured on our chitosan/PEO membranes compared to cells cultured on commercially available ThinCert® membranes, most likely due to the use of different cell seeding numbers (2.5 x 10^5 cells cm^{-2} for chitosan/PEO membranes; 1.5 x 10^5 cells cm^{-2} for ThinCert® membranes) and/or the different surface topographies of the two membrane types. Further increase in the cell seeding number or cultivation time to achieve potentially higher TEER values was not possible since this resulted in non-physiologic multilayer formation (BeWo cells are not contact inhibited). Therefore, the higher translocation of macromolecules and NPs across the placental BeWo monolayer on chitosan/PEO membranes might not only be the result of the higher permeability of the membranes (as evidenced by higher transfer across cell-free membranes) but different barrier properties might also partially account for the observed differences. Interestingly, Eom et al. also reported differences in TEER values during the formation of mouse brain endothelial monolayers (bEnd.3) on electrospun PCL fibers versus conventional flat porous membranes even with the same cell seeding number.[69] While TEER values for conventional membrane cultures peaked at 3 days of cultivation, they decreased to the same levels as for the electrospun membrane cultures at day 5.[69] Overall, further studies are warranted to understand in how far these differences in the TEER value could have an impact on paracellular transport. However, at least for NPs, predominant uptake pathways seem to involve endocytotic transcellular pathways rather than paracellular transfer routes. [70, 71]

The permeability of our chitosan/PEO membranes for a broad size-range of molecules and NPs (Na-F (0.3 kDa), FITC-Dextran (40 kDa), 25 nm PMMA, 70, 180 and 520 nm PS NPs) was evaluated across empty membranes and in presence of a confluent BeWo trophoblast barrier. It is known that substances below 500 Da can cross the placenta easily, while larger substances are transported at a much lower or slower rate or are even completely retained.[32, 72] Translocation studies with both chitosan/PEO and commercial track etched PET membranes mostly reproduced the expected relative size-dependent transport of diffusion markers and NPs through the BeWo trophoblast barriers. However, a few interesting things could be observed. First, absolute transfer rates for 40 kDa FITC-Dextran and all the NPs were significantly higher when chitosan/PEO membranes were used, highlighting the superior permeability of the newly developed electrospun membranes compared to track etched polymer membranes. Second, the apical concentrations of the 180 nm NPs (for chitosan/PEO) and the 520 nm PS NPs (for both membranes) decreased much more than what was observed for the 70 nm PS NPs. A possible explanation for these findings might be an increased cellular uptake of the larger NPs. Indeed, CLSM images showed an increased NP fluorescence after exposing BeWo cells to 180 nm PS NPs, while no obvious differences between the 70 nm and 520 nm PS NPs could be observed. However, CLSM imaging is a rather qualitative way of analysis and more sensitive detection methods should be implemented in future studies to investigate

quantitative NP uptake in a more reliable manner. Another explanation could also be a different sedimentation and/or agglomeration behavior of the different NPs, which has to be addressed in future studies. Finally, the 180 nm PS NPs showed higher transfer rates than the 70 nm PS NPs when the chitosan/PEO membranes were used. At first glance, these results may contradict the previously described size-dependent placental PS NP transport[47]. However, the 70 nm and 180 nm PS particles, although supplied by the same manufacturer, could have slight differences in surface characteristics or other NP properties that may influence translocation rates or the interaction of the NPs with the different membranes. For example, zeta potential measurements in PBS showed that the 180 nm PS NPs exhibited a more negative surface charge than the 70 nm PS NPs, and the hydrodynamic size of the 180 nm PS NPs in PBS was even smaller than the hydrodynamic size of the 70 nm PS NPs (185.8 vs 224.4 nm, respectively). These observations indicate that there could be other differences apart from NP size that could influence NP transfer rates.

Currently, the best method to verify the predictive value of an in vitro translocation model and avoid species-specific uncertainties is to compare the obtained results with data collected in highly predictive human ex vivo models, where the transport of exactly the same NPs across an entire human organ can be investigated. Therefore, we conducted human ex vivo placenta perfusion studies with few selected NPs due to the low throughput and limited access to human placentas. 25 nm PMMA and 70 nm PS NPs were chosen since for larger PS NPs, only very limited placental transfer was observed.[47] The results revealed that the in vitro model with the chitosan/PEO membranes well approximated the values obtained from ex vivo perfusion of human term placentas, while translocation rates determined with commercial track-etched PET membranes considerably underestimated placental transfer in particular for the larger NPs where the membrane itself constituted a major barrier to the free transfer of the particles. A high sensitivity of in vitro transfer models to detect even a minor transfer of potential toxicants is paramount to proper risk assessment, in particular when it comes to placental transfer and the protection of the highly sensitive developing fetus.

Nevertheless, CLSM images showed that some of the larger NPs were also absorbed in the chitosan/PEO membranes, which could potentially hamper predictive NP transport studies. However, the NP-membrane interactions became negligible in relevant experimental conditions in the presence of a confluent cell layer as the cells largely reduced the direct contact of the NPs with the membranes. This effect was evidenced in CLSM micrographs, demonstrating that the larger NPs were taken up by the BeWo cells but revealed only very few particles in the membrane itself. The observed uptake and accumulation of NPs by trophoblast cells is well in line with previous findings from placenta perfusion studies (summarized in [44]), and highlights the importance to not only consider the direct toxicity of translocated particles but also potential indirect fetotoxic effects mediated by NP interference with placental tissue function and signaling processes relevant to fetal wellbeing.[45]

Conclusions

To advance in vitro biobarrier models, current research efforts largely focus on the improvement of the biological models (e.g. from cell lines to primary cells or from single cells to co-cultures) or to recreate a dynamic microenvironment (e.g. microphysiological chips) while little attention is paid to the membranes. Here, we successfully developed novel, free-standing electrospun chitosan/PEO membranes which are readily permeable to a broad size range of molecules and NPs. The chitosan/PEO membranes outperformed commercial track-etched polymer membranes in regards to delivering more predictive translocation rates in particular for high molecular weight molecules and NPs. Moreover, the nanofibrous structure more closely mimics the natural ECM, which together with the high porosity might decisively improve cell-cell interactions and communication. While this study focused on the barrier translocation using a single cell layer, further experiments using co-culture biobarrier models are needed to understand if chitosan/PEO membranes could also allow more physiologic effect studies. Moreover, it would be interesting to integrate the novel chitosan/PEO membranes in a microfluidic chip to investigate whether highly permeable electrospun membranes in combination with dynamic exposure conditions can further push the predictive power of in vitro biobarrier models. This is of particular importance for studies of NP-biobarrier interactions because NPs exhibit unique transport kinetics as well as agglomeration and sedimentation behaviors, and a dynamic microenvironment can reproduce a more predictable particle exposure, dosage and cellular uptake.[68, 73, 74] Furthermore, a liquid flow has been shown to induce a more relevant cell morphology and glucose transport in placenta-on-chip devices.[24, 25]

Overall, the highly permeable electrospun membranes provide an important contribution to the improvement of human relevant in vitro models, which ultimately supports risk assessment of NPs and contributes to the reduction of animal experimentation.

Experimental Methods

Polymer solution preparation

For the electrospinning, polymer solutions with a total polymer concentration of 4% were prepared by dissolving chitosan (degree of deacetylation 85% and viscosity 50 mPa s; Heppe Medical Chitosan GmbH 24503) and poly(ethylene oxide) (Sigma 182028) with a molecular weight of 600 kDa in 90% acetic acid (Sigma 695092) using ultrapure water (MilliQ, > 18 MΩ cm). The chitosan:PEO ratio of 95:5 was chosen to obtain membranes with the highest possible chitosan content in combination with stable spinning conditions. The solutions were mixed overnight at ambient conditions on a magnetic stirrer until homogenous mixtures were obtained. Electrospinning took place within 48 h after solution preparation to prevent aging effects and polymer degradation.

Polymer solution characterization

The viscosity of the polymer solution was determined as a function of shear rate on a Physica MCR 300 rheometer (Anton Paar, Buchs, Switzerland) with cone-plate geometry (CP50-1). To measure the flow curves, shear rates were varied from 0.01 to 1000 s^{-1}.

The conductivity of the spinning solution was determined with a conductometer from Mettler Toledo (SevenCompact Duo pH/Cond S213, Switzerland) equipped with a Pt 100 dip-type conductometric cell (c = 0.83 cm^{-1}).

Electrospinning

The membranes were directly electrospun on cell culture inserts. To do so, the original membrane of ThinCert® cell culture inserts (Greiner Bio-One, 665631) was cut away with a scalpel. A liquid PDMS solution (Sylgard® 184 PDMS) was prepared (base reagent/cross linker ratio 10:1) and the cell culture insert was dipped in the solution for 1 sec to deposit a thin film of PDMS on it (the purpose was to glue the electrospun membrane tightly to the insert). The cell culture insert with PDMS was placed on a metal collector plate attached to a negative potential, which served as the counter electrode collecting the fibers. The rest of the electrospinning setup consisted of a 2 mL plastic syringe containing the chitosan/PEO solution to be ejected by an infusion pump (World precision instruments, Sarasota, FL, USA) at a constant flow rate of 7 µL min^{-1} through a blunt-ended needle (21G x 7/8", Braun, Melsungen, Germany), which served as the positive electrode. The needle tip of the syringe was placed 18 cm above the cell culture insert and a voltage of +12 kV and -4 kV was applied respectively, generated by two voltage supply sources (AIP Wild AG, Oberglatt, Switzerland). To control the electrical field strength, LabView software (National Instruments, Austin, TX, USA) was used. The whole electrospinning process took place in a Faraday cage placed in a fume hood at ambient conditions.

Membrane crosslinking

Since as-spun chitosan/PEO fibers are highly soluble in acidic solutions and water, they need to be stabilized before experiments in aqueous environments can be performed. This was achieved by chemical crosslinking in glutaraldehyde vapor.[36, 75] 4 mL of aqueous GA (50% in H$_2$O; Sigma G7651) were added to a desiccator (1 dm^3 volume). Then, the cell culture inserts with the membranes were placed on the desiccator plate above the liquid and the membranes were allowed to crosslink for 4 h. Afterwards, the membranes were dried in a vacuum oven for at least 24 h at 40 °C to remove any unreacted GA residues.

Scanning electron microscopy

SEM images of the electrospun membranes were taken with a Hitachi S-4800 (Hitachi High-Technologies, Canada) scanning electron microscope. To facilitate sample preparation, the membranes used for SEM imaging were not glued with PDMS,

but only loosely deposited on the cell culture inserts during electrospinning. Prior to imaging, a conductive double-sided carbon tape was affixed to a SEM stub and a free-standing chitosan/PEO membrane was brought into contact with the sticky top of the carbon tape. Since this made the membrane stick to the SEM stub, the membrane could finally be peeled off from the insert by gently pulling on it. Afterwards, the samples were sputter coated with 7 nm of gold/palladium (LEICA EM ACE600) to reduce electron charging effects. SEM images were acquired at an accelerating voltage of 2 kV and current flow of 10 µA.

Determination of fiber diameter & pore size

Fiber diameter and pore size of chitosan/PEO membranes were determined from SEM images. For all investigated conditions (2 min and 4 min electrospun membranes), SEM images from 6 different membranes produced on 3 different days and imaged at 2 different positions were analyzed using the Fiji ImageJ software.[76] Mean fiber diameters were determined from ~100 individual measurements of fiber diameters per image. Pore size was determined by measuring the Feret diameter of all the pores present in the respective microscopy images (SEM images with a higher magnification of 8k were used for this purpose). To do so, the shape of each pore was manually reconstructed using the "Polygon" tool and the Feret diameter was measured via the measurement tool.

Thickness & porosity measurements

Due to inherent fluorescent properties of the chitosan/PEO membranes, it was possible to reconstruct their 3D structure using a confocal laser scanning microscope (CLSM 780, Zeiss, Feldbach, Switzerland) equipped with a 488 nm laser. Inserts with electrospun membranes were embedded with Mowiol® 4-88 (Sigma-Aldrich 81381) on microscopy slides. Mowiol was dried over night at 40 °C and membranes were cut off from the holder with a scalpel. CLSM z-stack images were acquired, which allowed us to reconstruct the 3 dimensional structure of the membranes. With these 3D representations, the thickness of the electrospun membranes could be determined. To determine the porosity of chitosan/PEO membranes, maximum intensity projections were created from the z-stack images. The resulting images were segmented in Fiji ImageJ and the porosity was calculated with Equation (1):

$$porosity = \frac{total\ pore\ area}{membrane\ area} * 100\% \qquad (1)$$

For both thickness and porosity measurements, 6 different chitosan/PEO membranes produced on 3 different days were analyzed, and each membrane was analyzed at 2 different positions.

The porosity of commercially available ThinCert® membranes was calculated based on data supplied by the manufacturer, assuming a pore size of 3 µm, a pore density of 2 x 10^6 pores cm^{-2} and a growth area of 113,1 mm^2 with Equation (2):

$$porosity = \frac{total\ pore\ area}{membrane\ area} * 100\% \qquad (2)$$

where

$$total\ pore\ area = area\ of\ one\ pore * total\ number\ of\ pores$$

Water contact angle measurements

The hydrophilicity of the different membranes was determined by WCA measurements using a Krüss "Drop Shape Analyzer". Droplets of 2 μL were dispensed onto the scaffolds and the contact angle was determined by the ADVANCE software (Krüss) with the "lying drop" method using an elliptic fit.

Cell culture

BeWo b30 cells, a human placental choriocarcinoma cell line with cytotrophoblastic characteristics, were kindly provided by Prof. Dr. Ursula Graf-Hausner (Zurich University of Applied Sciences, Wädenswil, Zürich) with permission from Dr. Alan L. Schwartz (Washington University School of Medicine, MO, USA). The cells were cultured in Ham's F-12K medium (Gibco 21127) supplemented with 10% fetal bovine serum (FBS, Sigma-Aldrich F9665), 1% penicillin/streptomycin (Sigma P4458) and 2 mM L-Glutamine (Sigma G7513). The cells were cultivated in a humidified incubator at 37 °C with 5% CO_2 and sub-cultured twice a week using trypsin-EDTA solution (Sigma T3924). When cells were seeded on the different membranes for the experiments, another media was used, namely endothelial cell growth medium MV (PromoCell, C-22220) supplemented with 1 vial Supplement Mix (PromoCell, C-39225) according to the manufacturer's instructions (PromoCell, Heidelberg, Germany) and 1% penicillin/streptomycin, which will be referred to as endothelial cell medium (EC media). This medium was conveniently chosen as it is also compatible with endothelial cells[32] and allows an easy expansion to co-culture models in future studies

Cell cultivation on commercial and electrospun membranes

Electrospun chitosan/PEO membranes or commercially available PET ThinCert® cell culture inserts (pore size 3 μm, pore density 2 x 10^6 pores cm^{-2}, growth area 1.131 cm^2; Greiner Bio-One 665631) were pre-coated with 200 μL of 50 μg mL^{-1} collagen type IV from human placenta (Sigma-Aldrich C5533, Buchs, Switzerland) on the apical and basolateral side for 1h at 37 °C / 5% CO_2. Afterwards, the membranes were washed three times with PBS (Sigma-Aldrich D8537). For cytotoxicity (LDH and MTS) assays, 1.5 x 10^5 BeWo cells in 500 μL EC media were added to the apical side of each membrane insert, and 1.5 mL of EC media was added basolaterally. The cells were cultured for 24 h or 3 days at 37 °C / 5% CO_2 in EC media (medium change after 48h) under static conditions. For all other studies, 1.5 x 10^5 cells in 500 μL EC media were added to the apical side of the ThinCert® membranes and 2.5 x 10^5 cells in 500 μL EC media to

the apical side of the chitosan/PEO membranes and cultivated at 37 °C / 5% CO_2 (medium change after 48 h).

Cytotoxicity assays

To assess cell viability of BeWo cells and exclude potential cytotoxic effects of the novel chitosan/PEO membranes, MTS (3-(4,5-dimethylthiazol-2-yl)-5-(3-cyrboxymethoxy-phenyl)-2-(4-sulfophenyl)-2H-tetrazolium, inner salt) assays and LDH assays were conducted after 24 h and 96 h of cell culture. 1 h before conducting the assays, 50 μL of a 2% Triton-X100 solution (Sigma-Aldrich T8787) was added to the apical compartment of a control insert to lyse the cells (total Triton-X100 concentration 0.2%). Then, 3 x 50 μL media of each apical and basolateral sample were pipetted to a 96 well plate. For the MTS assay, 100 μL of Cell-Titer96 Aqueous One Solution (Promega G3581) were added to each insert and incubated for 3 h at 37°C / 5% CO_2. Afterwards, the apical and basolateral media from each insert were combined to adjust for permeability differences and 3 x 200 μL of each sample were pipetted to a 96 well plate for absorbance measurements at 490 nm with a microplate reader ($Mithras^2$ LB 943, Berthold Technologies GmbH, Zug, Switzerland). To calculate cell viability, corrected sample absorbance values were first determined (absorbance of the sample minus absorbance of cell free control). Then, viability was calculated using Equation (3), where the control condition was cells cultured on commercial ThinCert® membranes:

$$(3)\ Cell\ Viability\ [\%] \\ = corrected\ sample\ absorbance \\ /\ mean\ absorbance\ of\ control\ condition$$

For the LDH assay, the CytoTox96® Non-Radioactive Cytotoxicity Assay kit (Promega G1781) was used according to the manufacturer's instructions. In brief, assay reagent was added to each well with the previously collected media supernatants and the 96 well plates were incubated at room temperature (RT) for 30 min in the dark. After 30 min, stop solution was added and absorbance was measured with the Mithras microplate reader at 490 nm.

To calculate the total LDH release of each insert, absorbance values from both apical and basolateral compartment were summed. Cytotoxicity was then calculated as relative LDH release of cells cultured on chitosan membranes compared to cells grown on commercial ThinCert® membranes according to Equation (4):

$$(4)\ Relative\ LHD\ release \\ = corrected\ sample\ absorbance \\ /\ mean\ absorbance\ of\ control\ condition$$

Transepithelial electrical resistance

To evaluate barrier formation, TEER measurements were performed after 1, 2, 3 and 4 days using a chopstick electrode (STX3, World Precision Instruments Inc., Sarasota, USA). TEER was measured on the collagen-coated chitosan/PEO and ThinCert® membranes in the presence or absence of cells. To obtain TEER values for the cell layer, the intrinsic resistance of the membrane (TEER measured on inserts without cells) was subtracted from the total resistance (membrane with cells). The values were corrected for the surface area (Ω cm^{-2}).

Sodium fluorescein (Na-F) and FITC-Dextran exclusion assays

To assess barrier formation, exclusion of Na-F and 40 kDa FITC-Dextran was determined after 3 days and 4 days of cell culture. To do so, 0.5 mL of a 5 μM Na-F (Sigma-Aldrich, F6377) or 40 kDa FITC-Dextran (Sigma-Aldrich, FD40S) solution in phenol red-free EC media was added to the apical compartment and 1.5 mL phenol red-free EC media to the basal chamber. Inserts were incubated for 3 h at 37 °C / 5% CO$_2$. Afterwards, 3 x 50 μL of each basolateral sample were pipetted to a 96 well plate and the amount of Na-F and FITC-Dextran were detected by fluorescence measurements using a microplate reader (Mithras^2 LB 943, Berthold Technologies GmbH, Zug, Switzerland) at an excitation wavelength of 489 nm and emission of 525 nm.

Immunocytochemistry (ICC)

ICC staining was performed to verify that tight cell layers covered the whole membrane. Cells cultured on chitosan/PEO or ThinCert® membranes for 3 days were fixed in 4% paraformaldehyde (PFA; Sigma-Aldrich 16005, Buchs, Switzerland) in buffered PBS (Sigma-Aldrich D8537) / 0.2% Triton X-100 (Sigma-Aldrich T8787) for 10 min at RT and washed three times with PBS. Inserts were stored at 4 °C until staining was performed. Inserts were first blocked in 5% goat serum (Sigma-Aldrich, G6767) in PBS at 37 °C for 30 min. Then, primary rat-anti-tubulin (Abcam ab6161, Cambridge, UK; 1:1000) and mouse-anti-(γ)-catenin (BD biosciences 610253, Allschwil, Switzerland; 1:500) or mouse-anti-ZO-1 (Invitrogen 339100, Frederick, MD, USA; 1:100) diluted in 0.5% bovine serum albumin (BSA; Sigma-Aldrich A9647) in PBS were applied for 60 min at RT (tubulin, γ-catenin) or overnight at 4 °C (ZO-1). Inserts were washed three times with PBS and incubated with Alexa Fluor A488 goat anti-mouse (Invitrogen A-11029, Eugene, OR, USA; 1:400) and Alexa Fluor A555 goat anti-rat (Invitrogen A21434, Eugene, OR, USA; 1:400) (tubulin, γ-catenin staining) or A488 goat anti-mouse (Invitrogen A11029, Eugene, OR, USA; 1:400) (ZO-1 staining) diluted in 0.5% BSA in PBS for 1 h at RT. Inserts were washed three times with PBS, and during the second washing step, 40,6-diamidin-2-phenylindol (DAPI; Sigma-Aldrich D9542, Buchs, Switzerland; 1:1000 dilution in PBS) was included for 10 min at RT.

Whole inserts were embedded with Mowiol® 4-88 (Sigma-Aldrich 81381) on microscopy slides. Mowiol was dried over night at 40 °C and membranes were cut off from the holder with a scalpel. An Axio Imager 2 (Zeiss, Feldbach, Switzerland) was used to obtain images from the whole membrane area, while a confocal laser scanning microscope (CLSM 780, Zeiss, Feldbach, Switzerland) was used to take high resolution images and z-stacks.

hCG ELISA

To measure hCG production in cells cultured on chitosan/PEO membranes or ThinCert® inserts in the presence or absence of 20 μM forskolin (Sigma F6886), ELISA assays were conducted. Cells were cultured on the membranes for 3 days in EC media before 20 μM forskolin was added. After 24 h, supernatants from the apical and basolateral compartments were pooled and stored at -80 °C until further use.

High protein binding 96 well plates (Corning costar 9018) were coated with polyclonal rabbit anti-human chorionic gonadotropin (Dako, A0231) in 50 mm NaHCO$_3$ (1:1000 dilution) at 4 °C overnight, while the plates were sealed with sealing tape (Thermo Fisher Scientific, 232701). The next day, the plates were washed three times with 0.1% Tween-20 in PBS and blocking was performed with 1% BSA (Sigma A9647) at RT for 2 h. Afterwards, plates were washed again three times with 0.1% Tween 20 in PBS before standard or supernatants were added for 90 min at 37 °C. For the standard curve, hCG (Antibodies.com, HOR-250) concentrations of 0-6'000 pg mL^{-1} were used (serial dilutions in 1% BSA in PBS) and the samples were diluted in 1% BSA in PBS (1:10 dilution for untreated samples, 1:100 dilution for forskolin treated samples). After three washing steps, mouse anti-hCG (Serotec, MCA1436) was diluted in 1% BSA in PBS (1:5'000) and added to the wells for 90 min at 37 °C. Five washing steps with 0.1% Tween-20 in PBS were performed, and the wells were incubated with goat anti-mouse-IgG-horse radish peroxidase conjugate (BioRad #1706516) diluted in 1% BSA in PBS (1:5000) for 90 min at 37 °C. Plates were washed five more times and 100 μL peroxidase substrate (3,3',5,5'-Tetramethylbenzidine (TMB) Liquid Substrate System; Sigma T8665) were added to each well for 15 min at RT. Absorbance was measured at 370 nm with a microplate reader (Mithras^2 LB 943 Monochromator Multimode Reader, Berthold Technologies, Zug, Switzerland). Concentration linearity for the standards was given between 0 and 6000 pg mL^{-1}.

NP dispersion and characterization

Fluorescently labelled NPs of different sizes were commercially obtained. 25 nm PMMA micromer® greenF particles were available from Micromod (29-00-251). 70 nm and 180 nm yellow fluorescent PS-Particles (FP-00552-2 and FP-0252-2, Spherotech Inc., Lake Forest, IL, USA) were delivered as a 1% w/v suspension in 0.02% sodium azide as preservative. 520 nm fluorescent carboxylated PS microspheres were obtained in 2.5% aqueous suspensions from Polysciences (Fluoresbrite® Carboxylate YG 0.50 Microspheres, 15700-10). Stock particle solutions were vortexed before each use, diluted in EC media and immediately added to the cells. To characterize the

particles, their hydrodynamic diameter was measured at 100 μg mL^{-1} (70 nm, 180 nm and 520 nm PS particles) or 1'000 μg mL^{-1} (25 nm PMMA) in 10% PBS and EC media (Zetasizer Nanoseries, nano-ZS90, Malvern, Worcestershire, UK). Additionally, zeta potential measurements were performed from 100 μg mL^{-1} (70 nm, 180 nm and 520 nm PS particles) or 1'000 μg mL^{-1} (25 nm PMMA) dilutions in 10% PBS (Zetasizer Nanoseries, nano-ZS90, Malvern, Worcestershire, UK).

Particles were also imaged with SEM. To do so, 50 μL of each particle suspension was pipetted on an adhesive carbon tape previously mounted on a SEM stub. Particles were sputter coated with a 10 nm thick gold/palladium layer before imaging. Images were taken on a FEI Quanta 650 ESEM at an accelerating voltage of 5 kV (70 nm PS) or 3 kV (180 nm PS, 520 nm PS). The 25 nm PMMA particles could not be detected in the SEM.

Translocation studies

The translocation of differently sized molecules and NPs across the placental barrier was investigated after 3 days of cell culture. Transfer studies were done with 5 μM Na-F, 5 μM 40 kDa FITC-Dextran, 500 μg mL^{-1} 25 nm PMMA NPs and 50 μg mL^{-1} of the 70 nm, 180 nm and 520 nm PS particles in phenol red-free EC media. The molecules and NPs were added to the apical compartment and cells were incubated at 37 °C / 5% CO$_2$. After 0, 0.25, 2, 4, 6, 8 and 24 h, samples were collected (10 μL from the apical compartment and 50 μL from the basolateral compartment) in a 96 well plate. The apical samples were diluted in 40 μL phenol red-free EC media. After sample collection, basolateral media was renewed by adding 50 μL fresh medium to each insert. To determine the amount of molecules or particles in the samples, fluorescent signals of the samples were measured at an excitation wavelength of 475 nm and an emission of 525 nm with a microplate reader (Mithras^2 LB 943, Berthold Technologies GmbH, Zug, Switzerland).

At each time point, the transported amount of molecules and particles (ΔQ_n) in the basolateral compartment was calculated and corrected for the amount of samples taken before (Equation 5):

$$\Delta Q_n = C_n * V_w + \sum_{j=1}^{n-1} V_s * C_j \qquad (5)$$

where C_n is the concentration measured at time t_n, V_w is the volume of the well (1.5 mL) and V_s is the sample volume. The sum of the sample amount removed during previous time points is added as well (Σ). Results were then expressed as basolateral amount or concentration of the initial dose in %. Equilibrium between the apical and basolateral chamber would be reached if 75% of the applied molecules/particles would pass the cell layer and could be found in the basolateral compartment.

NP uptake & absorption

After NP translocation studies, cells were fixed in 4% paraformaldehyde (Sigma-Aldrich 16005, Buchs, Switzerland) / 0.2% Triton X-100 (Sigma-Aldrich T8787) for 10 min at RT and

washed three times with PBS (Sigma-Aldrich D8537). Then, cells were blocked in 5% goat serum (Sigma-Aldrich, G6767) in PBS at 37 °C for 30 min. Phalloidin Alexa Fluor® 633 (Invitrogen A22284) diluted 1:50 in 0.5% BSA (Sigma-Aldrich A9647) in PBS was applied for 60 min at RT. Afterwards, the membranes were washed three times with PBS, and during the second washing step, 40,6-diamidin-2-phenylindol (DAPI; Sigma-Aldrich D9542, Buchs, Switzerland; 1:1000 dilution in PBS) was included for 10 min at RT.

Whole inserts were embedded with Mowiol® 4-88 (Sigma-Aldrich 81381) on microscopy slides. Additionally, cell-free membranes were also embedded after the transport studies in Mowiol® 4-88. Mowiol was dried over night at 40 °C and membranes were cut off from the holder with a scalpel. A confocal laser scanning microscope (CLSM 780, Zeiss, Feldbach, Switzerland) was used to take high quality images and z-stacks to determine NP uptake into the cells and adsorption to the membranes.

Ex vivo human placenta perfusion

The project was ethically approved and the expecting mothers gave their informed written consent to the subsequent use of their placentas after delivery. Placentas from uncomplicated pregnancies were obtained from the Kantonsspital St. Gallen after planned caesarean sections. Maternal and fetal vessels of an intact cotyledon were cannulated and perfused in a closed system as described previously.[77, 78] Briefly, M199 tissue culture media (for 70 nm PS perfusion) or DMEM (for 25 nm PMMA perfusion) was diluted with Earl s buffer (1:2) and supplemented with BSA (10 g L^{-1}), dextran 40 (10 g L^{-1}), sodium bicarbonate (2.2. g L^{-1}), glucose (1 g L^{-1}, not added for PMMA perfusions), amoxicillin (250 g L^{-1}) and sodium heparin (2500 IU L^{-1}) to obtain the perfusion medium (PM) (all reagents were purchased from Sigma-Aldrich, Buchs, Switzerland). To assure a good quality of the obtained data, experiments were only considered valid when the pre-perfusion did not show any signs of leakage, the fluid transport from the fetal to the maternal side was lower than 4 mL h^{-1} throughout the experiments and the pH remained between 7.2 and 7.4. For NP translocation studies, 25 nm PMMA (25 μg mL^{-1}) and 70 nm PS (25 μg mL^{-1}) particles were added to the maternal circuit and fetal and maternal samples were taken after 0, 0.25, 0.5, 1, 2, 3, 4 and 6 h. The samples were centrifuged at 800 rpm to remove residual erythrocytes and the amount of NPs was determined by fluorescence measurements at 485 nm excitation and 528 nm emission in a microplate reader (BioTex FLx800, Witec AG).

Statistical analysis

Statistical analysis was done in R software.[79] Statistical differences between three or more groups were assessed using one-way ANOVA followed by a Tukey's Honest Significant Difference post-hoc test. Statistical differences between mean values of two groups were assessed using a Welch's two sample t-test. P-values < 0.05 were considered statistically significant.

Data availability

Generated and/or analyzed datasets from this study are available from the corresponding author on reasonable request.

Author Contributions

Conflicts of interest

There are no conflicts to declare.

Acknowledgements

References

1. N. Strambeanu, L. Demetrovici and D. Dragos, in *Nanoparticles' Promises and Risks: Characterization, Manipulation, and Potential Hazards to Humanity and the Environment*, eds. M. Lungu, A. Neculae, M. Bunoiu and C. Biris, Springer, 2015, DOI: 10.1007/978-3-319-11728-7_2, pp. 9-19.

2. M. Hoover, D. Myers, L. J. Cash, R. Guilmette, W. Kreyling, G. Oberdorster and R. Smith, *Radiation Safety Aspects of Nanotechnology*, United States, 2017.

3. T. Rönkkö and H. Timonen, *Journal of Alzheimer's Disease*, 2019, **72**, 15-28.

4. W. J. Stark, P. R. Stoessel, W. Wohlleben and A. Hafner, *Chem. Soc. Rev.*, 2015, **44**, 5793-5805.

5. X. He and H.-M. Hwang, *J. Food Drug Anal.*, 2016, **24**, 671-681.

6. S. Raj, S. Jose, U. S. Sumod and M. Sabitha, *J. Pharm. Bioallied Sci.*, 2012, **4**, 186-193.

7. M. Mozafari, J. Rajadas and D. L. Kaplan, in *Nanoengineered Biomaterials for Regenerative Medicine*, eds. M. Mozafari, J. Rajadas and D. Kaplan, Elsevier, 2019, DOI: https://doi.org/10.1016/B978-0-12-813355-2.00001-6, pp. 1-11.

8. *Official Journal of the European Union*, 2011, **L275**, 38-40.

9. H. Gavilán, S. K. Avugadda, T. Fernández-Cabada, N. Soni, M. Cassani, B. T. Mai, R. Chantrell and T. Pellegrino, *Chem. Soc. Rev.*, 2021, **50**, 11614-11667.

10. H. C. Davis, S. Kang, J.-H. Lee, T.-H. Shin, H. Putterman, J. Cheon and M. G. Shapiro, *Biophys. J.*, 2020, **118**, 1502-1510.

11. D. Pouliquen, J. J. Le Jeune, R. Perdrisot, A. Ermias and P. Jallet, *Magn. Reson. Imaging*, 1991, **9**, 275-283.

12. P. H. Hoet, I. Brüske-Hohlfeld and O. V. Salata, *J. Nanobiotechnol.*, 2004, **2**, 12-12.

13. E. Fröhlich and E. Roblegg, *Arch. Toxicol.*, 2016, **90**, 2297-2314.

14. R. Landsiedel, E. Fabian, L. Ma-Hock, W. Wohlleben, K. Wiench, F. Oesch and B. van Ravenzwaay, *Arch. Toxicol.*, 2012, **86**, 1021-1060.

15. Y. Zhou, Z. Peng, E. S. Seven and R. M. Leblanc, *Journal of Controlled Release*, 2018, **270**, 290-303.

16. A. M. Grabrucker, B. Ruozi, D. Belletti, F. Pederzoli, F. Forni, M. A. Vandelli and G. Tosi, *Tissue barriers*, 2016, **4**, e1153568-e1153568.

17. A. Pietroiusti, L. Campagnolo and B. Fadeel, *Small*, 2013, **9**, 1557-1572.

18. Z. Lan and W.-X. Yang, *Nanomedicine*, 2012, **7**, 579-596.

19. C. Muoth, L. Aengenheister, M. Kucki, P. Wick and T. Buerki-Thurnherr, *Nanomedicine*, 2016, **11**, 941-957.

20. H. F. Krug and P. Wick, *Angew Chem Int Ed Engl*, 2011, **50**, 1260-1278.

21. S. Grafmüller, P. Manser, H. F. Krug, P. Wick and U. von Mandach, *Journal of visualized experiments : JoVE*, 2013, DOI: 10.3791/50401, 50401.

22. S. Hirn, N. Haberl, K. Loza, M. Epple, W. G. Kreyling, B. Rothen-Rutishauser, M. Rehberg and F. Krombach, *Beilstein Journal of Nanotechnology*, 2014, **5**, 2440-2449.

23. M. P. Tibbe, A. D. van der Meer, A. van den Berg, D. Stamatialis and L. I. Segerink, in *Biomedical Membranes and (Bio)Artificial Organs*, WORLD SCIENTIFIC, 2017, vol. Volume 2, pp. 295-321.

24. C. Blundell, E. R. Tess, A. S. R. Schanzer, C. Coutifaris, E. J. Su, S. Parry and D. Huh, *Lab on a Chip*, 2016, **16**, 3065-3073.

25. J. S. Lee, R. Romero, Y. M. Han, H. C. Kim, C. J. Kim, J.-S. Hong and D. Huh, *The Journal of Maternal-Fetal & Neonatal Medicine*, 2016, **29**, 1046-1054.

26. B. J. van Meer, H. de Vries, K. S. A. Firth, J. van Weerd, L. G. J. Tertoolen, H. B. J. Karperien, P. Jonkheijm, C. Denning, A. P. Ijzerman and C. L. Mummery, *Biochemical and Biophysical Research Communications*, 2017, **482**, 323-328.

27. M. W. Toepke and D. J. Beebe, *Lab on a Chip*, 2006, **6**, 1484-1486.

28. J. D. Wang, N. J. Douville, S. Takayama and M. ElSayed, *Ann. Biomed. Eng.*, 2012, **40**, 1862-1873.

29. S. Dekali, C. Gamez, T. Kortulewski, K. Blazy, P. Rat and G. Lacroix, *Toxicology Reports*, 2014, **1**, 157-171.

30. I. George, S. Vranic, S. Boland, A. Courtois and A. Baeza-Squiban, *Toxicol. In Vitro*, 2015, **29**, 51-58.

31. P. Wick, A. Malek, P. Manser, D. Meili, X. Maeder-Althaus, L. Diener, P.-A. Diener, A. Zisch, H. F. Krug and U. v. Mandach, *Environ. Health Perspect.*, 2010, **118**, 432-436.

32. L. Aengenheister, K. Keevend, C. Muoth, R. Schönenberger, L. Diener, P. Wick and T. Buerki-Thurnherr, *Sci. Rep.*, 2018, **8**, 5388.

33. K. Feltz, E. Growney Kalaf, C. Chen, R. Scott Martin and S. Sell, *A review of electrospinning manipulation techniques to direct fiber deposition and maximize pore size*, 2017.

34. J. Rnjak-Kovacina and A. S. Weiss, *Tissue Engineering Part B: Reviews*, 2011, **17**, 365-372.

35. A. Nishiguchi, S. Singh, M. Wessling, C. J. Kirkpatrick and M. Möller, *Biomacromolecules*, 2017, **18**, 719-727.

36. P. Bösiger, G. Tegl, I. M. T. Richard, L. Le Gat, L. Huber, V. Stagl, A. Mensah, G. M. Guebitz, R. M. Rossi and G. Fortunato, *Carbohydr. Polym.*, 2018, **181**, 551-559.

37. P. J. VandeVord, H. W. T. Matthew, S. P. DeSilva, L. Mayton, B. Wu and P. H. Wooley, *J. Biomed. Mater. Res.*, 2002, **59**, 585-590.

38. T. Kean and M. Thanou, *Adv. Drug Del. Rev.*, 2010, **62**, 3-11.

39. F. Ajalloueian, H. Tavanai, J. Hilborn, O. Donzel-Gargand, K. Leifer, A. Wickham and A. Arpanaei, *BioMed Research International*, 2014, **2014**, 475280.

40. T. Cunha, B. Teixeira, B. Santos, M. Almeida, G. Dias and J. das Neves, in *Chitosan-Based Systems for Biopharmaceuticals*, DOI: https://doi.org/10.1002/9781119962977.ch5, pp. 75-92.

41. F. Croisier and C. Jérôme, *Eur. Polym. J.*, 2013, **49**, 780-792.

42. M. Pakravan, M.-C. Heuzey and A. Ajji, *Polymer*, 2011, **52**, 4813-4824.

43. T. Notter, L. Aengenheister, U. Weber-Stadlbauer, H. Naegeli, P. Wick, U. Meyer and T. Buerki-Thurnherr, *Translational Psychiatry*, 2018, **8**, 193.

44. L. Aengenheister, R. R. Favaro, D. M. Morales-Prieto, L. A. Furer, M. Gruber, C. Wadsack, U. R. Markert and T. Buerki-Thurnherr, *Placenta*, 2021, **104**, 199-207.

45. B. B. Dugershaw, L. Aengenheister, S. S. K. Hansen, K. S. Hougaard and T. Buerki-Thurnherr, *Part. Fibre Toxicol.*, 2020, **17**, 31.

46. T. Buerki-Thurnherr, K. Schaepper, L. Aengenheister and P. Wick, *Chem. Res. Toxicol.*, 2018, **31**, 641-642.

47. P. Wick, A. Malek, P. Manser, D. Meili, X. Maeder-Althaus, L. Diener, P.-A. Diener, A. Zisch, F. Krug Harald and U. von Mandach, *Environ. Health Perspect.*, 2010, **118**, 432-436.

48. S. Grafmueller, P. Manser, L. Diener, P.-A. Diener, X. Maeder-Althaus, L. Maurizi, W. Jochum, F. Krug Harald, T. Buerki-Thurnherr, U. von Mandach and P. Wick, *Environ. Health Perspect.*, 2015, **123**, 1280-1286.

49. A. Schmidt, D. M. Morales-Prieto, J. Pastuschek, K. Fröhlich and U. R. Markert, *J. Reprod. Immunol.*, 2015, **108**, 65-71.

50. R. N. Carter, S. M. Casillo, A. R. Mazzocchi, J.-P. S. DesOrmeaux, J. A. Roussie and T. Gaborski, R. , *Biofabrication*, 2017, **9**, 015019.

51. C. Jud, S. Ahmed, L. Müller, C. Kinnear, D. Vanhecke, Y. Umehara, S. Frey, M. Liley, S. Angeloni, A. Petri-Fink and B. Rothen-Rutishauser, *BioResearch Open Access*, 2015, **4**, 457-468.

52. V. S. LeBleu, B. MacDonald and R. Kalluri, *Experimental Biology and Medicine*, 2007, **232**, 1121-1129.

53. R. Jayadev and D. R. Sherwood, *Curr. Biol.*, 2017, **27**, R207-R211.

54. H. Takahashi-Iwanaga, T. Iwanaga and H. Isayama, *Archives of Histology and Cytology*, 1999, **62**, 471-481.

55. G. A. Abrams, S. L. Goodman, P. F. Nealey, M. Franco and C. J. Murphy, *Cell and Tissue Research*, 2000, **299**, 39-46.

56. A. Pozzi, P. D. Yurchenco and R. V. Iozzo, *Matrix Biol.*, 2017, **57-58**, 1-11.

57. M. J. Mondrinos, Y.-S. Yi, N.-K. Wu, X. Ding and D. Huh, *Lab on a Chip*, 2017, **17**, 3146-3158.

58. L. Cartwright, M. S. Poulsen, H. M. Nielsen, G. Pojana, L. E. Knudsen, M. Saunders and E. Rytting, *International journal of nanomedicine*, 2012, **7**, 497-510.

59. M. R. Feneley and G. J. Burton, *Placenta*, 1991, **12**, 131-142.

60. C. J. P. Jones, L. K. Harris, J. Whittingham, J. D. Aplin and T. M. Mayhew, *Placenta*, 2008, **29**, 215-219.

61. E. Bongaerts, L. Aengenheister, B. B. Dugershaw, P. Manser, M. B. J. Roeffaers, M. Ameloot, T. S. Nawrot, H. Bové and T. Buerki-Thurnherr, *J. Nanobiotechnol.*, 2021, **19**, 144.

62. L. Aengenheister, D. Dietrich, A. Sadeghpour, P. Manser, L. Diener, A. Wichser, U. Karst, P. Wick and T. Buerki-Thurnherr, *J. Nanobiotechnol.*, 2018, **16**, 79.

63. H. Juch, L. Nikitina, S. Reimann, M. Gauster, G. Dohr, B. Obermayer-Pietsch, D. Hoch, K. Kornmueller and R. Haag, *Nanotoxicology*, 2018, **12**, 90-103.

64. A. King, L. Thomas and P. Bischof, *Placenta*, 2000, **21**, S113-S119.

65. K. Orendi, M. Gauster, G. Moser, H. Meiri and B. Huppertz, *Reproduction*, 2010, **140**, 759-766.

66. K. Orendi, V. Kivity, M. Sammar, Y. Grimpel, R. Gonen, H. Meiri, E. Lubzens and B. Huppertz, *Placenta*, 2011, **32**, S49-S54.

67. H. Li, B. van Ravenzwaay, I. M. C. M. Rietjens and J. Louisse, *Arch. Toxicol.*, 2013, **87**, 1661-1669.

68. M. S. Poulsen, E. Rytting, T. Mose and L. E. Knudsen, *Toxicol. In Vitro*, 2009, **23**, 1380-1386.

69. S. Eom, S. M. Park, S. J. Han, J. W. Kim and D. S. Kim, *RSC Advances*, 2017, **7**, 38300-38306.

70. M. Sousa de Almeida, E. Susnik, B. Drasler, P. Taladriz-Blanco, A. Petri-Fink and B. Rothen-Rutishauser, *Chem. Soc. Rev.*, 2021, **50**, 5397-5434.

71. J. Zhao and M. H. Stenzel, *Polymer Chemistry*, 2018, **9**, 259-272.

72. M. R. Syme, J. W. Paxton and J. A. Keelan, *Clin. Pharmacokinet.*, 2004, **43**, 487-514.

73. C. Grabinski, M. Sharma, E. Maurer, C. Sulentic, R. Mohan Sankaran and S. Hussain, *Nanotoxicology*, 2016, **10**, 74-83.

74. A. C. Rinkenauer, A. T. Press, M. Raasch, C. Pietsch, S. Schweizer, S. Schwörer, K. L. Rudolph, A. Mosig, M. Bauer, A. Traeger and U. S. Schubert, *Journal of Controlled Release*, 2015, **216**, 158-168.

75. J. D. Schiffman and C. L. Schauer, *Biomacromolecules*, 2007, **8**, 594-601.

76. J. Schindelin, I. Arganda-Carreras, E. Frise, V. Kaynig, M. Longair, T. Pietzsch, S. Preibisch, C. Rueden, S. Saalfeld, B. Schmid, J.-Y. Tinevez, D. J. White, V. Hartenstein, K. Eliceiri, P. Tomancak and A. Cardona, *Nat. Methods*, 2012, **9**, 676-682.

77. S. Grafmüller, P. Manser, H. F. Krug, P. Wick and U. von Mandach, *JoVE*, 2013, DOI: doi:10.3791/50401, e50401.

78. L. Aengenheister, B. B. Dugershaw, P. Manser, A. Wichser, R. Schoenenberger, P. Wick, M. Hesler, Y. Kohl, S. Straskraba, M. J. F. Suter and T. Buerki-Thurnherr, *Eur. J. Pharm. Biopharm.*, 2019, **142**, 488-497.

79. R. C. Team, *Journal*, 2020.